Journal of Mines, Metals and Fuels, *71(11): 2222-2228; 2023. DOI: 10.18311/jmmf/2023/36051*

Print ISSN : 0022-2755

Journal of Mines, Metals and Fuels

**Contents available at:** *www.informaticsjournals.com/index.php/jmmf*

# Facile Synthesis of Spinel Zinc Aluminate Using Biofuel for Effective Photocatalytic Dye Degradation and Electrochemical Sensor Studies

**K. Gurushantha[1]*, K. Keshavamurthy[2], S. Shashidhar[3] and S. Meena[4]**

*[1]Department of Chemistry, M. S. Ramaiah Institute of Technology, Bengaluru - 560054, Karnataka, India; gurushanthak2016@gmail.com*

*[2]Department of Physics, Dayananda Sagar College of Engineering, Bengaluru - 560111, Karnataka, India; keshav.m85@gmail.com*

*[3]Department of Chemistry, New Horizon College of Engineering, Bengaluru - 560103, Karnataka, India; Shashidharchem32@gmail.com*

*[4]Department of Chemistry, Dayananda Sagar College of Engineering, Bengaluru - 560111, Karnataka, India*

## Abstract

*Zinc aluminate nanomaterial provide a potential candidate for photocatalytic and sensor applications. Using biofuel (banana peel powder), zinc aluminate was synthesized by SCM (solution combustion method) in the current study. The properties of the phase structures, chemical composition, morphologies, and photocatalytic sensors were characterized by utilizing powder X-ray diffraction, scanning electron microscope, CH analyzer, UV-Visible spectroscopy, and photocatalytic reactor. Indigo Carmine (IC) dye degradation under UV light was used to assess the photocatalytic activity. The results showed that zinc aluminate makes a superior photocatalyst for degrading organic dyes like indigo carmine. In a potassium hydroxide electrolyte medium, zinc aluminate was also an effective substance for paracetamol and lead metal sensing. The results confirm that the novel material could be used for various industrial applications.*

**Keywords:** *Photocatalysis, Sensors, $ZnAl_2O_4$*

## 1.0 Introduction

Zinc aluminate is a spinel-type oxide with excellent mechanical resistance, better stability towards thermal and chemical, a large surface area, and a narrowed band gap[1–3]. $ZnAl_2O_4$ spinel has found applications in ceramic industries due to its high catalytic performance. This nanomaterial as a catalyst, zinc aluminate spinel has been utilized in various processes, including hydrogenation, oil transesterification, hydroformylation, ethanol steam reforming, toluene degradation, and iso-butane combustion[4–8]. Foletto *et al.* reported that $ZnAl_2O_4$ nanocrystals are suitable for the photocatalytic degradation of Procion red dye in an aqueous media[9]. Fabian M *et al.* reported that chromium acidic black dye was degraded under UV light using zinc aluminate as a catalyst[10]. Para nitro phenol, Congo red, New Methylene Blue, Eosin B, Chicago Sky Blue, and Methyl Orange dyes were effectively degraded by zinc aluminate as a catalyst[11,12]. Synthesis of $ZnAl_2O_4$ nanocrystals by various methods has been reported recently. Han *et al.* reported that $ZnAl_2O_4$ nanowire synthesized by Melt-Injection Decomposition method using aluminum oxide and zinc nitrate at 350 °C for 5 hours[13]. Belyaev *et al.* reported that $ZnAl_2O_4$ powder by sol-gel method using boehmite sol precursors and zinc nitrate solution at 750 °C for 3 hours.

*Author for correspondence

Sommer *et al*. reported the pure phase of $ZnAl_2O_4$ at 1000 °C by direct spark plasma sintering route. Peillon reported that spinel $ZnAl_2O_4$ was synthesized by microwave oven using ZnO and $Al_2O_3$ precursors at 1350 °C[14].

All the above synthetic methods discussed require high temperature with a long reaction time, so we synthesize the zinc aluminate nanoparticles by solution combustion method with low temperature using green fuel banana peel powder within 15 minutes. The synthesized nanoparticles are used for the effective photocatalytic degradation of organic dyes and sensor applications.

## 2.0 Synthesis of Zinc Aluminate Nanoparticles (NPs)

The chemicals used in this investigation were procured from SD Fine Chemicals and were used directly without further purification. The precursors used for synthesis are zinc nitrate hexahydrate, aluminium nitrate hexahydrate, and banana peel powder. The solution combustion method was utilized to synthesize zinc aluminate with banana peel powder as a fuel. Freshly picked after ripening, the banana peel was dried in the open with sunlight for two days before being pulverized in a mortar and pestle. For the preparation of zinc aluminate, a stoichiometric amount of zinc nitrate hexahydrate, aluminium nitrate hexahydrate, and an optimum amount of banana peel powder was taken in a cylindrical pyrex dish; a small quantity of distilled water was added and then mixed well with the help of magnetic stirrer. The dish was placed into a preheated muffle furnace at about 500 °C. The solutions immediately start to boil, and large amounts of gasses are evolved due to the decomposition of metal nitrates. The solution undergoes spontaneous combustion resulting in the powder form of the product. The product was calcinated at 700 °C for 3 hours.

## 3.0 Results and Discussion

### 3.1 XRD

In Figure 1, the $ZnAl_2O_4$ XRD is presented. The identified diffraction peaks position at 2$\theta$ are 31.3, 36.5, 44.5, 48.8, 55.2, 59.5, 65.1, 74.0, and 77.5 and are related to the (220), (311), (400), (331), (422), (511), (440), (620), and (533) planes of $ZnAl_2O_4$, respectively, through the JCPDS

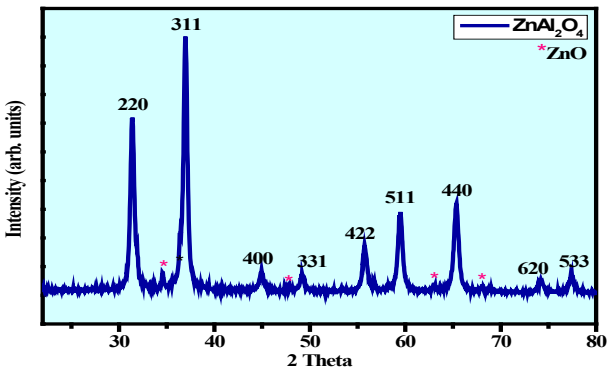


**Figure 1.** XRD of $ZnAl_2O_4$

card No. 05-0669, which confirms the formation of the $ZnAl_2O_4$. It can be seen that there are small impurities peaks of ZnO (JCPDS card No. 36–1451), which was similar to the results reported by Wang *et al*.[15]. The median crystalline size of the material was estimated as 16.0 nm by the Debye-Scherer's formula (1),

$$D = \frac{k\lambda}{\beta \cos\theta} \quad (1)$$

where D denotes the crystals average size, k denotes the Scherer's constant (k = 0.89), λ represents the wavelength of the X-ray source, β represents the diffraction peaks full-width half maximum, and θ denotes the Bragg angle.

### 3.2 Results of Energy Band Gap

The optical studies for $ZnAl_2O_4$ NPs were done by measuring the diffused reflectance spectral range of 200 to 800 nm, as depicted in Figure 2 (A). The Kubelka-Munk model was utilized to determine the connection between the diffuse reflectance (R) of prepared $ZnAl_2O_4$ nanoparticles (R), the scattering coefficient (S), with the absorption coefficient (K)[16].

The magnitude of 'n' signifies either a direct (n=1/2) or indirect (n=2) transition is permitted[17,18].

$$F(R) = \frac{(1-R)^n}{2R} = \frac{K}{S} \quad (2)$$

Energy band gap ($E_g$) values of synthesized $ZnAl_2O_4$ nanoparticles are measured by using Tauc equations (3 and 4), and a materials linear absorption coefficient ($\alpha$) is given by,

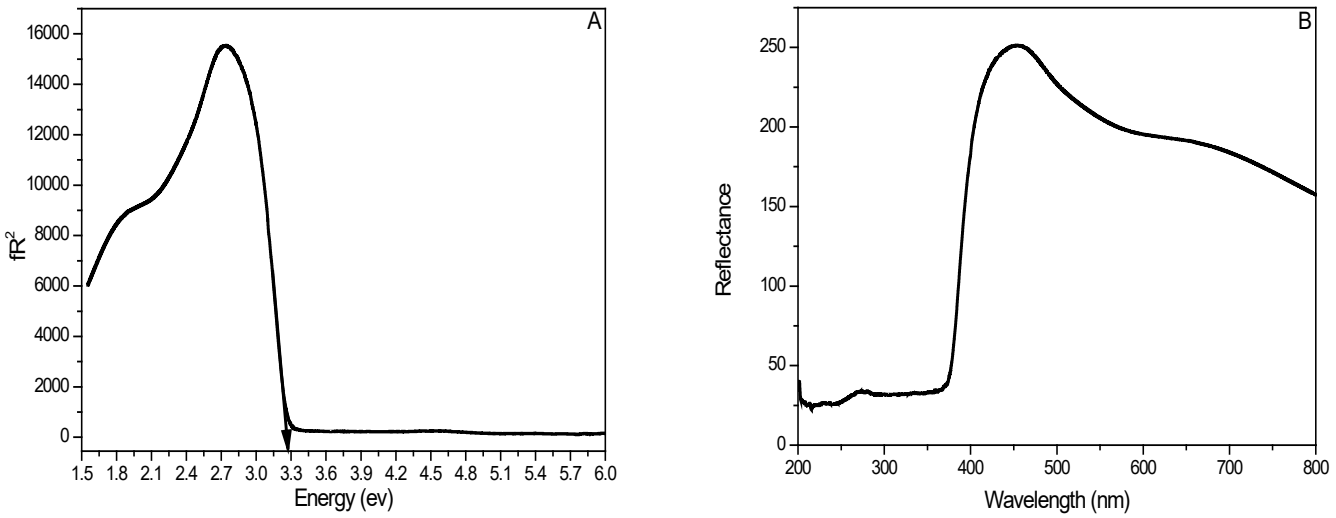


**Figure 2.** a) Band gap of $ZnAl_2O_4$ b) Reflectance spectra of $ZnAl_2O_4$ NPs.

$$\alpha = \frac{C_1\left(h\nu - E_g\right)^{\frac{1}{2}}}{h\nu} \quad (3)$$

$$[F(R)h\nu]^2 = C_2\left(h\nu - E_g\right) \quad (4)$$

The value of $E_g$ was calculated by extrapolating the linearly fitted regions to $[F(R)h\nu]^2=0$ from the $[F(R)h\nu]^2$ versus hν plot, and the band gap energy of synthesized $ZnAl_2O_4$ nanoparticles is 3.26 eV (Figure 2 (B)). The energy band gap for prepared nanoparticles is tuned compared to the $E_g$ of $ZnAl_2O_4$ available in the literature survey; the energy band gap decreased may be due to the fuel effect. The $E_g$ from results could relates the semiconductor activity of $ZnAl_2O_4$ NPs and its property precisely correlated to photocatalytic performance.

## 3.3 SEM

In Figure 3, $ZnAl_2O_4$ nanoparticles are shown in an SEM micrograph. Figure 3 displays that the particles are tightly agglomerated despite being porous. The particle grain size in the SEM micrograph measured from 82.25 to 161.67 nm. Also, the micrographs revealed identical-sized large and small particles. The constituents in nanomaterials were also confirmed by EDX analysis.

The EDX spectra of the $ZnAl_2O_4$ nanoparticles are depicted in Figure 4, in which it is clear that Zn, Al, and O elements are present. The area of the specimen that was chosen to record the EDX spectra is shown in the inset

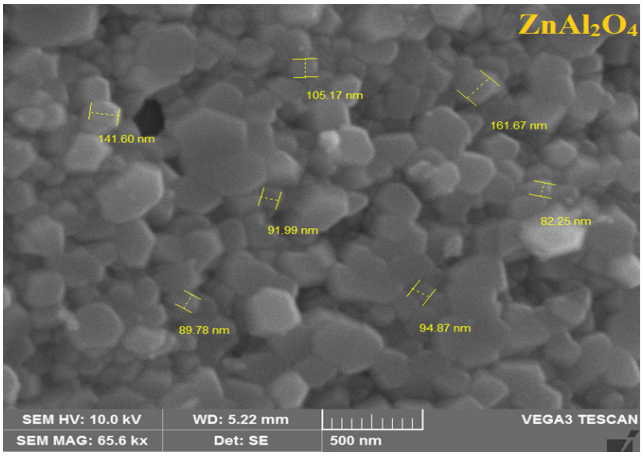


**Figure 3.** SEM micrograph of $ZnAl_2O_4$ nanoparticles.

of Figure 4. The atomic proportions of different cations in the $ZnAl_2O_4$ sample are enlisted in Table 1. The results display that the composition of material present and the

**Table 1.** The atomic proportions of various cations in the $ZnAl_2O_4$ sample.

| Element | Weight % | Atomic % |
|---|---|---|
| O | 28.62 | 51.20 |
| Zn | 43.22 | 18.93 |
| Al | 28.16 | 29.87 |

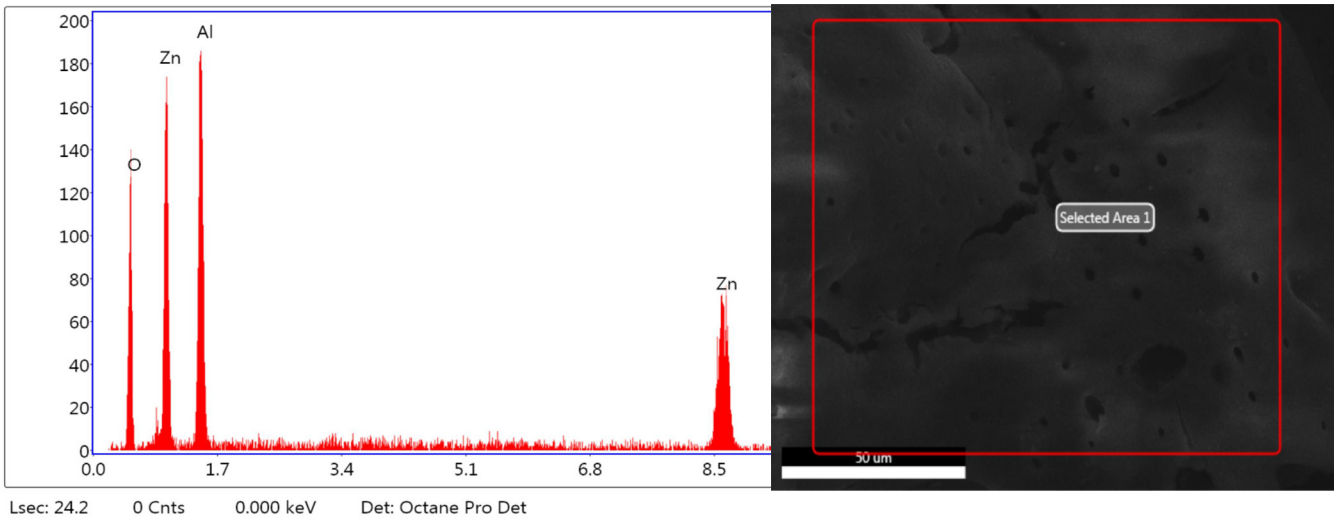


**Figure 4.** EDX spectra of the $ZnAl_2O_4$ nanoparticles (Inset Fig.: Selected area used to record the EDX spectra).

elemental analysis resulted from EDX has a reasonable degree of concordance. The produced material is in a pure phase because there is no trace of contamination. Furthermore, EDAX makes it clear that no ingredient is dissipated during annealing. The EDX measurement of nanoparticles may be impacted by their surface crystalline imperfections.

## 3.4 Photocatalytic Activity

Photocatalytic activity of synthesized $ZnAl_2O_4$ was conducted under UV light irradiation by taking IC as a model dye. The photodegradation of IC dye pollutant was determined by examining the absorbance at 611 nm during the experiment. Photodegradation of IC dye was conducted by taking respective stock solution (10 ppm) in 250 mL distilled water along with 50 mg of the photocatalyst $ZnAl_2O_4$ in a circular glass reactor. During the reaction, 4 mL of dye solution was taken out by pipetting, centrifuged and evaluate the absorbance using a UV-Visible spectrometer. As shown in Figure 5, IC dye concentration reduction in $ZnAl_2O_4$ photocatalysts under UV light was monitored every 15 minutes. The final results shows the degradation performance of $ZnAl_2O_4$ as photocatalyst on IC dye is increased over UV-light irradiation time, have incredible degradation performance in 75 min with 96 % (Figure 5).

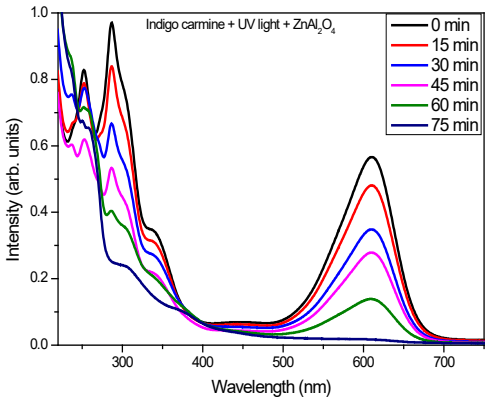


**Figure 5.** Absorbance spectra of IC dye

Under the action of UV radiation, the dye becomes photosensitized on the $ZnAl_2O_4$ photocatalyst surface. $ZnAl_2O_4$ was induced by UV light as electrons jumps from the Valence Band (VB) to the Conduction Band (CB), where they are excited and produce an equal amount of holes. The electrons produced in the CB are transported to the photocatalyst surfaces and stimulate the generation of superoxide radicals () by interacting with $O_2$. Correspondingly, water molecules and hydroxyl radicals are produced due to the holes in the VB. The produced radicals would break the IC dye into nontoxic by-products[19].

## 3.5 Electrochemical Studies

The Cyclic Voltammetry (CV) curves of $ZnAl_2O_4$ were shown in Figure 6(a) at different scanning rates in a 1.0 M KOH alkaline solution. The ideal rectangular forms of all

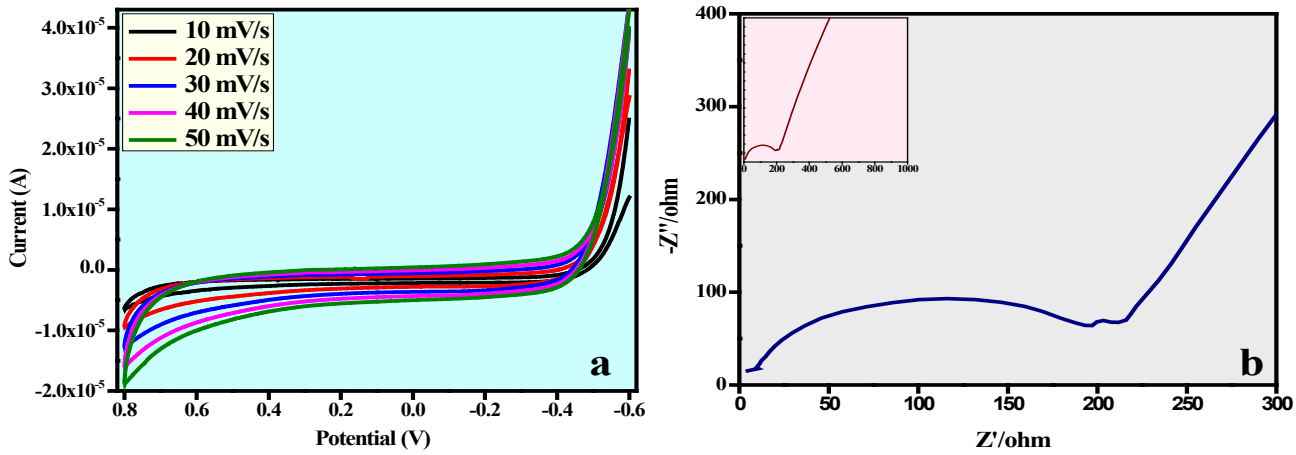


**Figure 6.** (a) CV curves of $ZnAl_2O_4$ at different scan rates. b) Nyquist plot of $ZnAl_2O_4$

the CV curves of potential within 0.8 V to -0.6 V, as seen in Figure 6(a), indicate a capacitive behaviour. As the scan rate rises, the peak current for each CV curve likewise grows and maintains a rectangular, symmetrical shape, demonstrating the stability of the curves. The specific capacitance (Cs) was calculated for $ZnAl_2O_4$ electrode of resulted CV plot using the following formula (5):

$$C_S = \frac{\int I \cdot dv}{v \times m \times \Delta V} \quad (5)$$

where $C_S$ (F/g), m (g) represents the mass of the $ZnAl_2O_4$ in the electrodes, I (A) denotes the current, v (mV/s) denotes the scanning rate, and ΔV (V) denotes the potential range. The calculated Cs of the $ZnAl_2O_4$ electrode is 16.7, 13.0, 11.2, 9.21, and 8.18 F/g. As the scanning rate increases, a capacitance declines possibly by the lesser penetration rate of ions from electrolyte within the electrode at a higher scanning rate[20].

The Nyquist plot of the $ZnAl_2O_4$ electrode is depicted in Figure 6(b). The high-frequency region from the

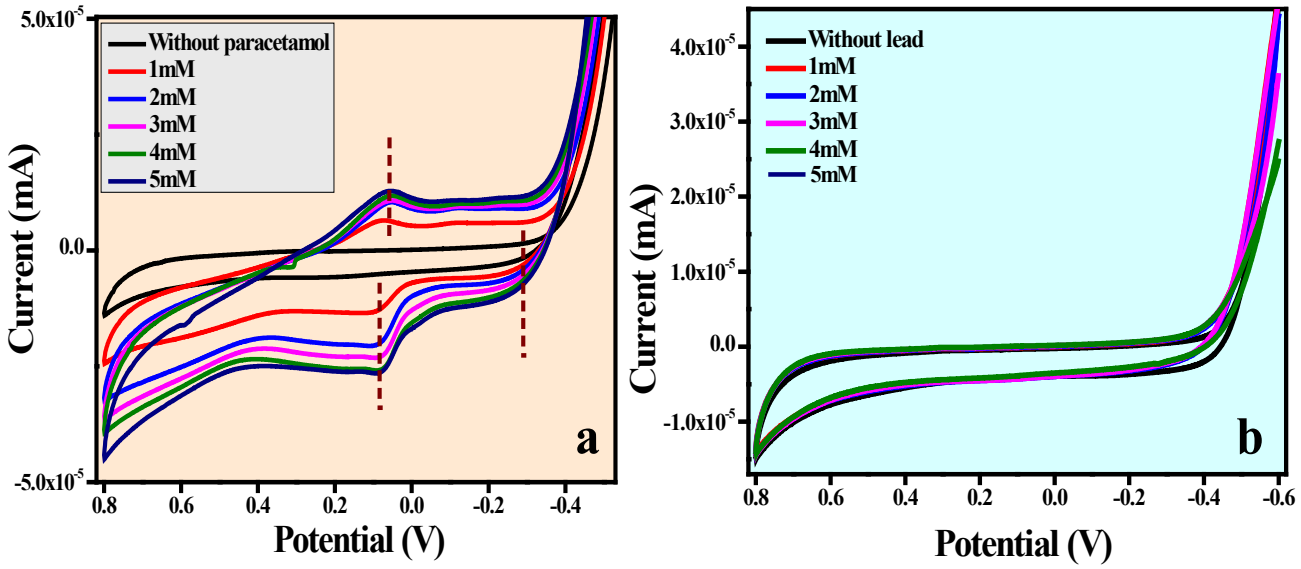


**Figure 7.** (a) CV plots of $ZnAl_2O_4$ electrode for detecting paracetamol, and (b) CV plots of $ZnAl_2O_4$ electrode for detecting Lead nitrate.

impedance curve has a semicircle, and in the low-frequency region, it has a straight-sloping line. The semicircles diameter correlates to the interfacial charge transfer resistance (Rct), that's also typically utilised to indicate the impedance of reactions happening at surface of electrode[21]. The curves yielded a 200Ω Rct resistance value, indicating that the $ZnAl_2O_4$ electrode exhibits excellent electrical conductivity. The electrolytic ions transfer resistance in the electrode pore and the low-frequency proton diffusion in electrode materials are shown by the straight line[21]. The ion diffusion processes are related with an angle with the real axis around 45° (Warburg impedance). This is one of the pseudocapacitance features usual characteristics.

### 3.6 Sensor Studies

The extension of electrochemical analysis for the $ZnAl_2O_4$ with graphite electrode for sensor features. On this view, the prepared electrode to sense the paracetamol in the 0.1 M KOH electrolyte. Figure 7 (a) explains CV analysis of the $ZnAl_2O_4$ electrode for sensing paracetamol of increasing concentration in the potential of – 0.6 V to + 0.8 V. In Figure 7 (a), the detection of paracetamol in KOH was validated by the new appearance anodic (0.06) and potential reduction peaks (0.085 and -0.29) at as compared to the bare electrolyte. The retention and sensitiveness were further ascertained by increasing the paracetamol quanity in the KOH by the electrode shown in Figure 7 (a). Hence we can conclude that $ZnAl_2O_4$ could act as a promising sensor electrode for paracetamol. Further, an attempt has been made to detect Lead nitrate in the electrolyte (Figure 7 (b)), but as there is no change in the CV peaks, we can conclude that the electrode could not be a sensor for Lead nitrate. Hence, in future work on the electrode, we are experimenting with the detection of Lead Nitrate in the different electrolytes.

## 4.0 Conclusion

In summary, nanomaterial $ZnAl_2O_4$ spinel was prepared by solution combustion method utilizing bio fuel banana peel powder. The median crystallite size of $ZnAl_2O_4$ nanoparticles is 16 nm, estimated using Debye-Scherer's formula. The band gap energy of synthesized $ZnAl_2O_4$ nanoparticles was evaluated by measuring reflectance and is found to be 3.26 eV. The photocatalytic activity of synthesized $ZnAl_2O_4$ catalyst has been evaluated; it is a suitable candidate for the pollutants degradation as indigo carmine dye under UV light. Also, $ZnAl_2O_4$ acts as a suitable sensor electrode for paracetamol determination. Hence the novelty of the nanomaterial and its applications was proved for upcoming multiple application.

## 5.0 References


1. Charinpanitkul T, Poommarin P, Wongkaew A, Kim K. Dependence of zinc aluminate microscopic structure on its synthesis. J Ind Eng Chem. 2009; 15:163–166. https://doi.org/10.1016/j.jiec.2008.09.017.
2. Ben Ayadi Z, El Mir L, Djessas K, Alaya S. Electrical and optical properties of aluminum-doped zinc oxide sputtered from an aerogel nanopowder target. Nanotechnology. 2007; 18:445702. https://doi.org/10.1088/0957-4484/18/44/445702.
3. Kong XY, Ding Y, Yang R, Wang ZL. Single-Crystal Nanorings Formed by Epitaxial Self-Coiling of Polar Nanobelts. Science. 2004; 303:1348–1352. https://doi.org/10.1126/science.1092356.
4. Galetti AE, Gomez MF, Arrúa LA, Abello MC. General Ni catalysts supported on modified $ZnAl_2O_4$ for ethanol steam reforming. Appl Catal A. 2010; 380:40–47. https://doi.org/10.1016/j.apcata.2010.03.024.
5. Lenarda M, Casagrande M, Moretti E, Storaro L, Frattini R, Polizzi S. Selective catalytic low pressure hydrogenation of acetophenone on Pd/ZnO/$ZnAl_2O_4$. Catal Lett. 2007; 114:79–84. https://doi.org/10.1007/s10562-007-9046-4.
6. Zawadzki M, Staszak W, Lopez-Suarez FE, Illan-Gomez MJ, Bueno-Lopez A. General Preparation, characterization and catalytic performance for soot oxidation of copper-containing $ZnAl_2O_4$ spinels. Appl Catal A. 2009; 371:92–98. https://doi.org/10.1016/j.apcata.2009.09.035.
7. Pugnet V, Maury S, Coupard V, Dandeu A, Quoineaud A, Bonneau JL, Tichit D. General Stability, activity and selectivity study of a zinc aluminate heterogeneous catalyst for the transesterification of vegetable oil in batch reactor. Appl Catal A. 2010; 374:71–78. https://doi.org/10.1016/j.apcata.2009.11.028.
8. Staszak W, Zawadzki M, Okal J. Solvothermal synthesis and characterization of nanosized zinc aluminate spinel used in iso-butane combustion. J Alloys Compd. 2010; 492:500–507. https://doi.org/10.1016/j.jallcom.2009.11.151.

9. Luiz E, Battiston S, Marimon J, Moro M, Severo L, Pereira F, *et al*. Synthesis of $ZnAl_2O_4$ nanoparticles by different routes and the effect of its pore size on the photocatalytic process. Microporous Mesoporous Mater. 2012; 163:29–33. https://doi.org/10.1016/j.micromeso.2012.06.039.
10. Fabian M, Elias A, Kostova N, Briančin J, Baláž P. Photocatalytic Activity of Nanocrystalline Gahnite ($ZnAl_2O_4$) Synthesized by Ball Milling. Proc 12th Int Multidiscip Sci Geo Conf. 2012; 491–498. https://doi.org/10.5593/sgem2012/s12.v3008.
11. Chaudhary A, Mohammad A, Mobin SM. Facile synthesis of phase pure $ZnAl_2O_4$ nanoparticles for effective photocatalytic degradation of organic dyes. Mater Sci Eng B. 2018; 227:136–144. https://doi.org/10.1016/j.mseb.2017.10.009.
12. Trisna A, Pradana S. An improved method for high photocatalytic performance of $ZnAl_2O_4$ spinel derived from layered double hydroxide precursor. SN Appl Sci. 2020; 2:842. https://doi.org/10.1007/s42452-020-2682-7.
13. Han D. Low-temperature synthesis and photoluminescence properties of oriented $ZnAl_2O_4$ nanowire arrays. Superlattices Microstruct. 2017; 111:1093–1098. https://doi.org/10.1016/j.spmi.2017.08.012.
14. Mehrotra RC, Singh A, Sogani S. Homo- and Heterometallic Alkoxides of Group 1,2, and 12 Metals. Chem Soc Rev. 1994; 23:215–225. https://doi.org/10.1039/CS9942300215.
15. Wang S, Sun G, Fang L, Lei L, Xiang X, Zu X. A comparative study of $ZnAl_2O_4$ nanoparticles synthesized from different aluminum salts for use as fluorescence materials. Sci Rep. 2015; 5:12849. https://doi.org/10.1038/srep12849.
16. Phys ZT. Ein Beitrag Zur Optik Der Farbanstriche. Z Techn Phys. 1931; 12:593–601.
17. Sinha R, Roy N, Rajasekhar R, Karnawat A, Mandal TK. N-doped carbon dot from cigarette-tobacco: Picric acid sensing in real water sample and synthesis of CD-MWCNT nano-composite for UV-photodetection. J Environ Chem Eng. 2021; 9:104971. https://doi.org/10.1016/j.jece.2020.104971.
18. Dhar S, Chakraborty P, Majumder T, Mondal SP. Acid Treated PEDOT: PSS Polymer and $TiO_2$ Nanorods Acid Treated PEDOT: PSS Polymer and $TiO_2$ Nanorods Schottky Junction Ultraviolet Photodetectors with Ultrahigh External Quantum Efficiency, Detectivity and Responsivity. ACS Appl Mater Interfaces. 2018; 10:41618–41626. https://doi.org/10.1021/acsami.8b12643.
19. Gurushantha K, Anantharaju KS, Kottam N, Keshavamurthy K, Ravikumar CR, Surendra BS, *et al*. Synthesis of $ZrO_2$: $Dy^{3+}$ Nanoparticles: Photoluminescent, Photocatalytic, and Electrochemical Sensor Studies. Adsorpt Sci Technol. 2022; 2022:5664344. https://doi.org/10.1155/2022/5664344.
20. Meena S, Anantharaju KS, Malini S, Arjun Dey, Renuka L, Prashantha SC, Vidya YS. Impact of temperature-induced oxygen vacancies in polyhedron $MnFe_2O_4$ nanoparticles: As excellent electrochemical sensor, supercapacitor and active photocatalyst. Ceram Int. 2021; 47:14723–14740.
21. Meena S, Anantharaju KS, Vidya YS, Renuka L, Malini S, Sharma SC, *et al*. $MnFe_2O_4/ZrO_2$ nanocomposite as an efficient magnetically separable photocatalyst with good response to Sunlight: Preparation, characterization and catalytic mechanism. SN Appl Sci. 2020; 2:328. https://doi.org/10.1007/s42452-020-2086-8.